Microfluid Nanofluid (2011) 11:307–316
DOI 10.1007/s10404-011-0797-2

RESEARCH PAPER

Aqueous droplet manipulation by optically induced Marangoni circulation

Wenqi Hu · Aaron T. Ohta

Received: 29 December 2010 / Accepted: 22 March 2011 / Published online: 8 April 2011

Abstract The manipulation of picoliter droplets is demonstrated using optically induced microscale circulatory flows. The circulation results from Marangoni effects induced by optical heating from light patterns created by a computer projector. Manipulation of single droplets and parallel manipulation of multiple droplets are achieved with induced forces of up to 1 nN and an average resolution of 146.5 μm.

Keywords Marangoni force · Thermocapillary flow · Droplet manipulation

1 Introduction

Droplets with picoliter volumes have wide application in biomedical assays (Srinivasan et al. 2004; Luo et al. 2006; Solvas et al. 2010). Further, as picoliter droplets are of a similar size as many types of cells, they are good candidates for modeling cellular behavior (Holden et al. 2007; Zagnoni and Cooper 2010) and for single-cell encapsulation (Choi et al. 2007; Di Carlo 2009; Hur et al. 2010). Droplets are also able to act as isolated reaction compartments that minimize cross contamination between samples and reagents (Song et al. 2006; Cygan et al. 2005).

Droplet manipulation has been demonstrated using mechanisms such as electrowetting (Chiou et al. 2008), dielectrophoresis (DEP) (Schwartz et al. 2004; Chiou et al. 2008; Park et al. 2008; 2010), and magnetic force (Zhao et al. 2010). Thermocapillary flow at liquid/liquid and liquid/air interfaces have also been used to manipulate droplets. The creation of thermal gradients is typically done using microfabricated heaters (Darhuber et al. 2003; Basu and Gianchandani 2009; Selva et al. 2010). Moving the droplets in pre-defined trajectories can be accomplished by performing droplet manipulation in microfluidic channels (Cordero et al. 2008; 2009; Emilie et al. 2009). The use of enclosed microfluidic channels limits the direct exposure of droplets to air, which can lead to evaporation (Farahi et al. 2005; 2006; Lereu et al. 2006; Passian et al. 2006). However, using an optothermal method to manipulate droplets in an immiscible medium in an open chamber can be preferable, as this method limits evaporation, and is capable of moving droplets in arbitrary, reconfigurable trajectories. For example, an infrared laser can be used to induce thermal Marangoni effects at a water/decanol interface, successfully manipulating water droplets (Kotz et al. 2004; Dixit et al. 2010). However, decanol is toxic, which is an issue if this system is to be used with cells. Thus, laser-induced droplet movement in a mineral oil–water system resulting from circulation was also explored (Dixit et al. 2010).

In this article, we report nano- and pico-liter droplet actuation by microscale circulation driven by optothermal Marangoni effects. Instead of using microstructured elements or lasers, a commercial computer projector is used to create temperature gradients by optical heating. The system described here uses an inexpensive microfluidic device that is highly programmable and capable of the parallel manipulation of multiple droplets, making it desirable for automated applications.

2 Theory

The presence of a temperature gradient will create thermocapillary flow at a liquid/air interface. The velocity field

W. Hu · A. T. Ohta (✉)
Department of Electrical Engineering,
University of Hawaii at Manoa, Honolulu, HI, USA
e-mail: aohta@hawaii.edu

between liquid layers induced by thermal Marangoni effects can be described as (Higuera 2000):

$$\eta\frac{\partial u}{\partial y} = \gamma\frac{\partial T}{\partial x}$$

where γ is the temperature derivative of the surface tension (N m^{-1} K^{-1}), η is the dynamic viscosity (kg m^{-1} s^{-1}), u is the velocity vector (m s^{-1}), and T is the temperature (K). For pure liquids, the temperature derivative γ can be derived using the Eötvös rule: $\gamma = -K_r/V_m^{2/3}$ (Eötvös 1886; Palit 1956), where V_m is the molar volume of the liquid and the constant $K_r = 2.1 \times 10^{-7}$ J K^{-1} mol$^{-2/3}$. Since surfactants are used in this experiment, the Eötvös rule is used here only to approximate the value of γ for qualitative analysis. This equation states that the shear stress on a surface is proportional to the temperature gradient (COMSOL Multiphysics 2008). In this research, the temperature gradient is optically controlled using the substrate to absorb energy from projected light.

The behavior of a droplet in response to thermally induced circulation can be modeled by coupling the Navier–Stokes equation, the heat-transfer equation, and the Marangoni effects at the liquid/air interface (Fig. 1). Fluid movement within the droplet is not considered, although the droplet thermal properties are taken into consideration. The droplet is treated as a solid sphere, and the oil/water interfacial thermocapillary effect is neglected. To prevent the simulated droplet from breaking the oil/air interface, a surface tension force is added to the model:

$$F_{surf} = P \times S_{cap} = \frac{2\gamma}{R} \cdot 2\pi Rh = 4\pi\gamma h = 4\pi\gamma(4\ \mu\text{m} - d)$$

where P is the pressure from Young's equation (Batchelor 2000), S_{cap} is the area of the hemispherical top of the droplet, R is the radius of the droplet, h is the height of the hemispherical top of the droplet, and d is the distance from the top of the droplet to the surface of the oil. In all the simulations, this surface tension force is only active when the top point of the droplet is within 4 μm from the surface of the oil.

The viscous force (F_{fluid}) and torque ($R \times F_{fluid}$) on the droplet are determined by integrating the stress tensor over the droplet surface. Based on these forces, both the displacement velocity and the rotational velocity of the droplet are determined. When the torque is considered in simulations, the motion of each point on the droplet is calculated by adding the effects of viscous force and torque. When the torque is ignored, only the viscous force is considered.

3D finite-element modeling was performed using COMSOL Multiphysics software. Figure 1a shows the simulation of the circulation in a 150-μm thick layer of FC-40 oil (3M Corporation) when a static heat source created by an optical pattern is present at the substrate/oil interface. To model the heat source, a saturated Gaussian temperature distribution with a peak temperature of 301 K and a full width at half maximum of 167 μm is set at the bottom boundary of the oil layer (Fig. 1c). This type of profile accurately models the light patterns produced by a computer projector in similar optical systems (Neale et al. 2009). The same type of saturated Gaussian profile is used to model temperature within the device, as temperature is proportional to absorption in the substrate, which in turn is directly proportional to light intensity. The environmental temperature is set to 300 K. The properties of the oil are: density = 1855 kg m^{-3}, absolute viscosity = 0.0041 centipoise, thermal conductivity = 0.0065 W m^{-1} K^{-1}, heat capacity = 1100 J kg^{-1} K^{-1} (3M Corporation, Fluorinert™ Electronic Liquid FC-40 material safety data sheet). The thermal properties of the droplet at room temperature are: density = 1000 kg m^{-3}, thermal conductivity = 0.58 W m^{-1} K^{-1}, heat capacity = 4180 J kg^{-1} K^{-1}. The surface tension at the liquid/air interface is set to 8.7 mN m^{-1}, and was measured by axisymmetric drop shape analysis (Zuo et al. 2007). Figure 1a shows half of the circulation pattern created by the static temperature profile of Fig. 1c. The highest velocity field is observed at the surface of the oil, bordering the center of the temperature gradient created by the heat source. This is due to the thermal Marangoni effect, which predicts that fluid flow arises due to temperature gradients. Further, larger temperature gradients produce flows with greater velocities. Another observation is that the circulation is axially symmetric. This feature can be used when the merging of separate droplets is required. When the heat source is translated in any direction, the circulation will no longer be symmetric. The simulation in Fig. 1b has a heat source that is moving along the x-axis at a rate of 300 μm s^{-1}, from a starting position centered about $x = 0$ μm. It can be seen that the streamlines are distorted, and the circulation on the trailing edge of the heat source is slower than in the case of a static heat source. The faster the heat source moves, the slower the circulation on the trailing edge. A comparison of the circulation velocities for the case of a static heat source and a moving heat source is shown in Fig. 1d. The asymmetry of the circulation should be taken into consideration when using a moving heat source to transport droplets.

The temperature profile of Fig. 1c is also used to simulate the results shown in Fig. 2. Both large and small droplets are initially positioned 200 μm away from the center of the heat-generating light pattern. In the opto-thermally induced circulation, large droplets will move towards to the center of the circulation above the light pattern (Fig. 2a), while small droplets are pushed away by the flow near the surface of the oil (Fig. 2b, d). This difference between large and small droplets is caused by the balance of viscous forces (Basu and Gianchandani 2009).

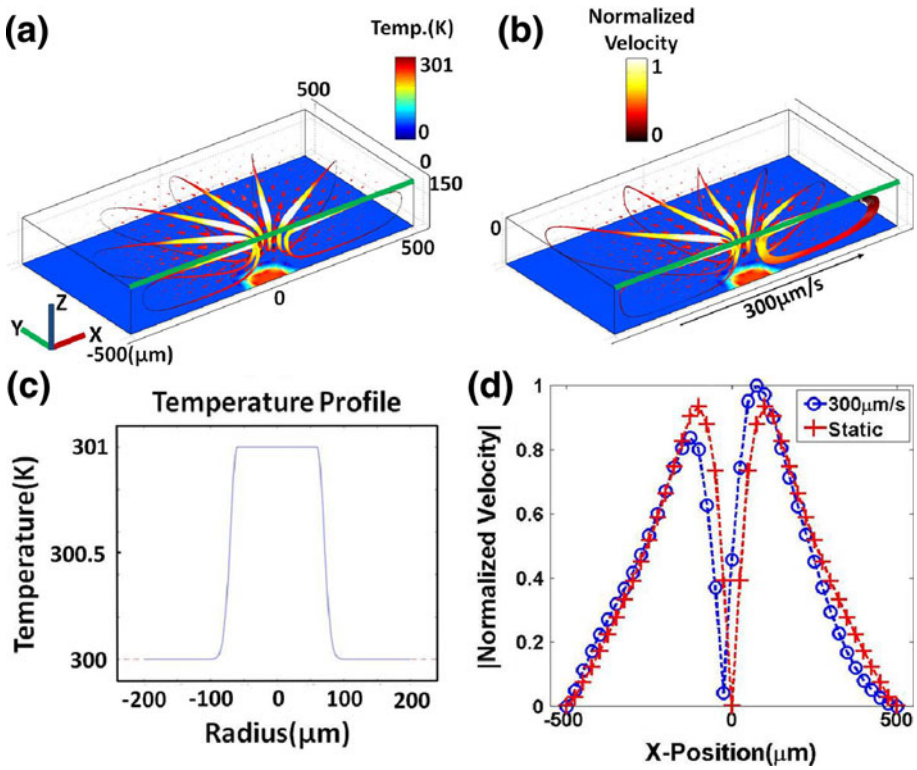

Fig. 1 Simulations of circulation in a 150-μm thick layer of FC-40 oil. **a** Circulation generated by a static heat source centered at $x = 0$ μm after 3 s. **b** Circulation generated by same heat source used in (**a**), moving to the right at a speed of 300 μm s^{-1} from an initial position centered at $x = 0$ μm. **c** The temperature profile used in the simulations shown in (**a**) and (**b**). **d** The magnitude of the circulation velocity along the *green* edges marked in (a) and (b)

For small droplets immersed in the upper flow (the flow moving away from the light pattern near the surface of the oil layer), the direction of the net viscous force on the droplet is directly outwards from the center of the light pattern. This makes the droplet follow the upper flow of the circulation, pushing the droplet away from the heat source. On the other hand, large droplets contact both the sub flow (the flow moving towards the light pattern, near the bottom of the oil layer) and the upper flow. As these two flows are in opposite directions, the viscous forces on the droplet arising from the upper and sub flows act against each other. When the viscous force from the sub flow dominates, the net force drags the droplet to the center of the light pattern. It should be noted that for the droplet to be pushed away, the circulatory flow should not be too strong, since this condition requires that the buoyancy force is larger than that of the downward vertical component of the viscous force, which occurs farther away from the center of the light pattern. If the circulation is strong, then the downward vertical component of the viscous force can push the droplet into the sub flow, causing it to move towards the center of the circulation. These qualitative descriptions will be more quantitatively discussed in Sect. 4.1. Finally, droplets with a radius less than 15% of the oil depth will circulate with the flow without being trapped. Stable droplet trapping is defined as the situation when a droplet is pulled towards the light pattern, and remains trapped in the center of the light pattern. This only occurs for droplets with radii greater than 15% of the oil depth.

In the research done by Basu and Gianchandani (2009), it was noted that the torque helps the droplet "roll" towards the circulation center. However, based upon the 3D simulations presented here, the torque has only a minor contribution to the overall droplet motion due to the circulation. This is shown more clearly by plotting the simulated x-displacement of the large droplet from the simulation shown in Fig. 2a for two cases: first, with the contribution of torque, and second, without the contribution of torque. The second case is a hypothetical situation that was not replicated experimentally, as it is difficult to decouple torque effects in a real system. Nevertheless, the simulated results of the two cases show only a small difference between the cases where torque is considered and where torque is ignored (Fig. 2c).

3 Materials and methods

The experimental setup is shown in Fig. 3. The light source is provided by a customized projector (Dell 2400MP with the projection optics removed). After being reflected by a mirror, the projected light pattern is focused by a long-working distance objective (5×). The absorbing substrate consists of a 1.1-mm thick glass slide coated with a 200-nm thick layer of indium tin oxide (ITO), followed by a 1-μm thick layer of amorphous silicon (a-Si), which absorbs light in the visible and UV wavelengths. The video data are recorded by a CDD camera (Pixelink-PLUB776U) mounted

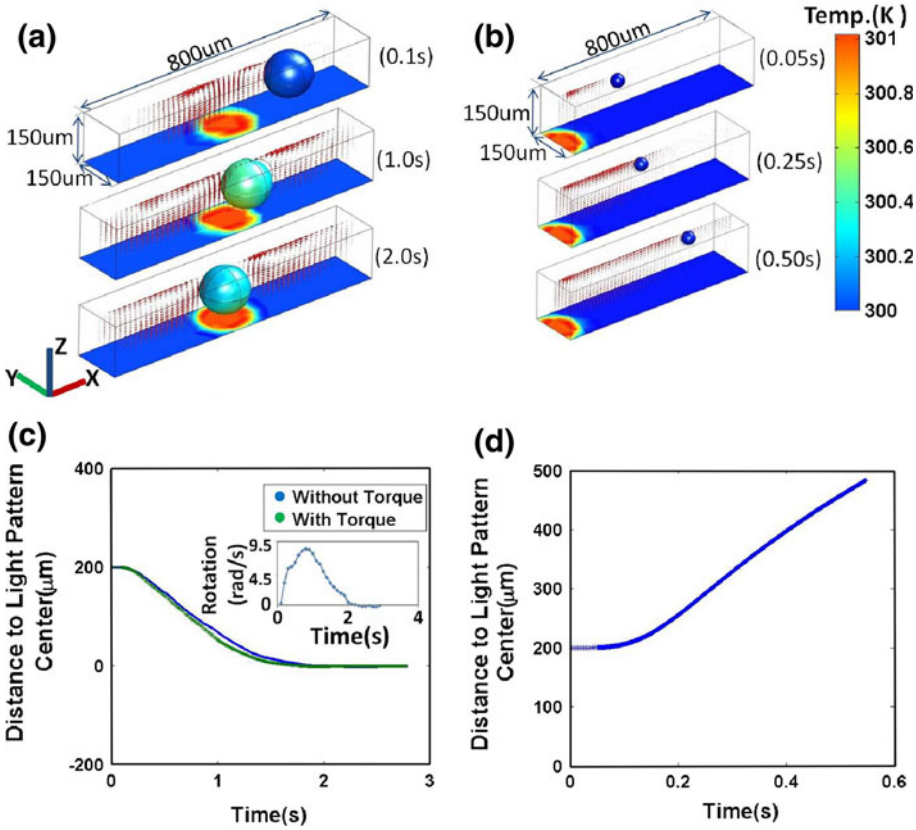

Fig. 2 Droplet movement due to circulation from optically induced thermal Marangoni force. Droplets are positioned 200 μm away from the center of the heat source, and the highest point of the droplet is 5 μm below the oil surface. **a** A large droplet (1.15 nl, radius: 65 μm) is dragged towards the center of light pattern by the circulatory flow. **b** A small droplet (33 pl, radius: 20 μm) is pushed away by the circulatory flow. **c** The distance between the center of the large droplet and the center of the heat source for the simulation in (**a**), with and without the contribution of torque on the droplet. The *inset* shows the rotation speed on the droplet when torque is considered as the droplet moves towards the center of the heat source. **d** The distance between the center of the small droplet and the center of the heat source for the simulation in (**b**)

on the upright microscope (Olympus BXFM). An open chamber (3 × 1.3 cm) was formed on the absorbing substrate using walls made out of polydimethylsiloxane (PDMS). The chemicals used in the experiments were: FC-40 fluorinated oil (3M Corporation), EA fluorinated surfactant (Rain Dance Technologies), RDT 1000 destabilizer (Rain Dance Technologies), and Tween 20 surfactant (Fisher Scientific). The droplet solution is created by mixing food dye (13.8% v/v) and Tween 20 (0.1% v/v) in deionized water. The carrier solution consists of FC-40 with 2% w/v RDT surfactant. The droplet solution is then mixed into the carrier solution (3.2% v/v). Droplets are obtained by shaking this solution. The fluorinated surfactant is used in our experiments to increase the stability of the oil/water interface (Holtze et al. 2008). The destabilizer solution used in the droplet fusion experiment is made by mixing RDT 1000 destabilizer (0.1% v/v) with FC-40. The temperature coefficient surface tension for the FC-40/air interface is given by $\gamma = -0.570$ mN m^{-1} K^{-1} according to the Eötvös rule. The force on a droplet is calculated using Stokes' Law:

$$F_d = 6\pi\eta R v$$

where F_d is the frictional force acting on the interface between the fluid and the particle (in N), η is the fluid viscosity (in kg m^{-1} s^{-1}), R is the radius of the spherical object (in m), and v is the particle's velocity (in m s^{-1}).

4 Results and discussion

4.1 Trapping of single droplets

The induced forces on single droplets using optically induced Marangoni circulation were characterized (Fig. 4). The radius of a droplet is measured by analyzing microscope images showing a top-down view of the droplet. The droplet volume is calculated from the measured radius by

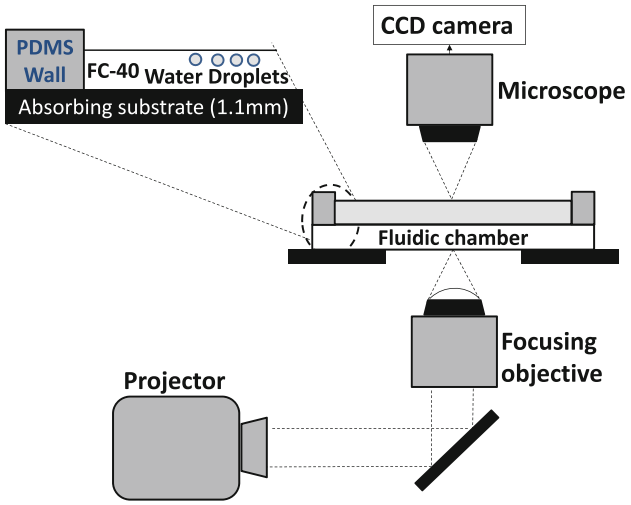

Fig. 3 Experimental setup. Light from the projector is focused on the absorbing substrate using a long-working distance 5× objective lens (Mitutoyo)

assuming a spherical droplet shape. Droplets used in the characterization experiments are positioned at a specific initial distance away from where a light pattern will be projected (Fig. 4a, 0 s). Velocity data are recorded thereafter. Since the droplet is obscured after its center passes over the edge of the light pattern, only the data where the center of the droplet is still detectable are used. The drag force from Stokes' Law is used to calculate force on the droplet. Positive and negative forces in the graphs in Fig. 4b, d, and e indicate that the droplets move away from and towards the light pattern, respectively. Experimental droplet behavior was similar to the simulated cases, where smaller droplets are pushed away from the light patterns, and larger droplets are attracted to and trapped by the light patterns (Fig. 4a). Here, the smaller droplet has a volume of 65 pl (radius: 25 μm), and the larger droplet has a volume of 556 pl (radius: 51 μm). This size-dependent droplet behavior is shown in more detail in Fig. 4b. The mechanism for the size dependence is the profile of the circulatory flow. As the velocity of the upper flow is larger compared with the sub flow, conservation of liquid flux dictates that the upper flow must be less than 50% of the total oil depth. Simulations with oil thicknesses less than 500 μm show that the thickness of the upper flow accounts for approximately 30% of the whole oil depth. This percentage decreases when the velocity of the upper flow increases. This flow profile affects how droplets of various sizes move in response to the optically induced circulation.

Droplets with radii less half than the thickness of the upper flow, or approximately 15% of the oil depth, either continuously circulate with the flow, or are pushed away from the light patterns. This is demonstrated by the droplet with a radius of 25 μm in Fig. 4b. This droplet continuously moves away from the light pattern, indicated by the positive values of force and velocity.

When the droplet radius approaches the thickness of the upper flow, or approximately 30% of the oil depth, the viscous force of upper and sub flow begins to balance each other. This behavior is demonstrated by the droplet with a radius of 38 μm in Fig. 4b. This droplet radius is approximately 30% of the oil depth of 130 μm. Instead of being pushed away, this droplet stays at the same location when the circulation is present.

When the droplet radius is larger than the thickness of the upper flow, or greater 30% of the oil depth, the droplet begins to be attracted to, and eventually trapped, by the light pattern. This is demonstrated by the decrease in the velocity of the 48-μm radius droplet after 1.3 s, showing that as the droplet moves closer to the center of the light pattern, it becomes trapped. This is shown more clearly by plotting the distance of the droplet from the center of the light pattern as a function of time for the 48-μm radius droplet (Fig. 4c). After 1.8 s, the droplet is completely within the area of the light pattern, making it difficult to detect droplet position. However, after this time point, the droplet remains within the area of the light pattern. If the light pattern is switched off, then the droplet position is near the center of the area that was illuminated.

The intensity and size of the light pattern also have an effect on droplet manipulation (Fig. 4d, e). In Fig. 4d, the radius of the droplet (43 μm) is larger than 30% of the overall oil depth (110 μm), so it moves towards the light pattern. The decrease in the magnitude of the force at low intensities (here 6.72 and 8.11 W cm^{-2}) is caused by weak circulatory flow, which provides only a small viscous force. The decrease in the magnitude of the force at high intensities (here 13.11 and 13.53 W cm^{-2}) is due to friction from the substrate, as the droplet contacts the substrate under strong convective flow. During experiments when the intensities are larger than 12.80 W cm^{-2}, corresponding to a very strong circulation, droplets are observed to move around bumps on the substrate, indicating that they are in contact with the lower surface.

Another empirical observation is droplets with radii between 15 and 30% of the oil depth can be controllably trapped. Figure 4e shows that by increasing the light pattern size, the scale and intensity of the circulation are successfully modulated to capture a small droplet (volume: 75 pl, radius: 26 μm, 20% of the oil depth) in a relatively large oil depth (130 μm). Smaller light patterns correspond to less total optical power, resulting in slower circulatory flows. Larger light patterns increase the total optical power, increasing circulatory flow velocity. Thus, the droplet is pushed away from the optical pattern with increasing speed as the pattern size increases from a radius of 39 to 79 μm. The decrease in velocity for the 113-μm radius light pattern

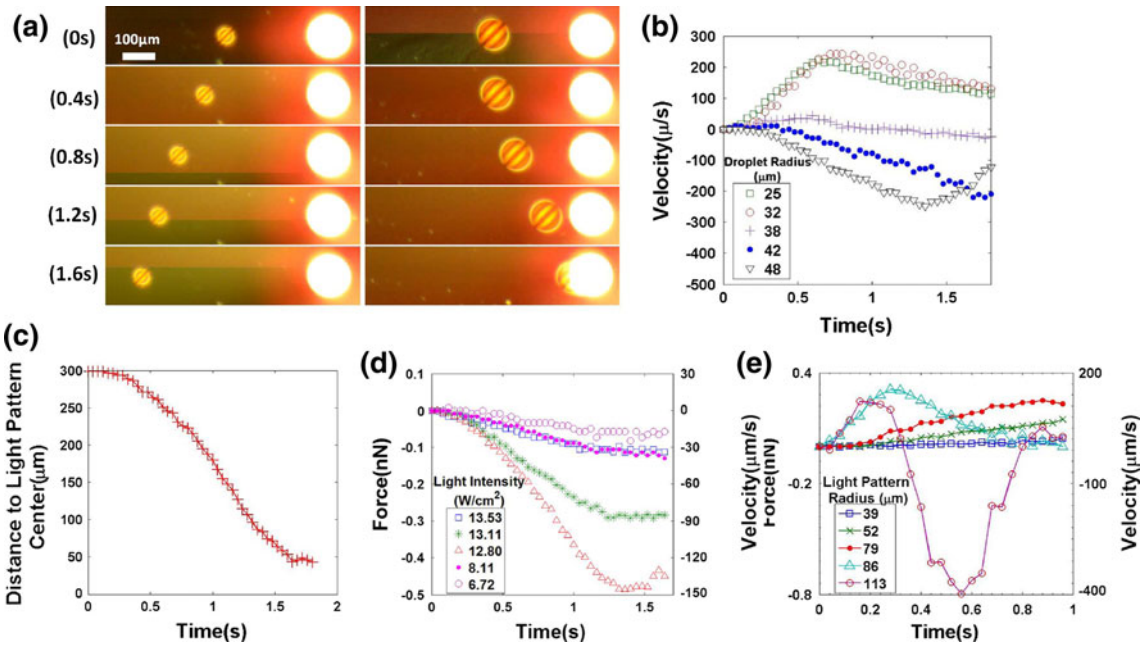

Fig. 4 Characterization of optothermal droplet manipulation. **a** Droplet capture experiment for small (65 pl, radius: 25 μm) and large (556 pl, radius: 51 μm) droplets. The initial distance between the droplet and the center of the light pattern is 300 μm (±5%), and the oil depth is 130 μm. **b** Induced force on droplets as a function of time for various droplet sizes (light pattern radius: 69 μm, oil depth: 130 μm). The initial distance between the droplet and the center of the light pattern is 300 μm (±5%), and light pattern intensity is 13.53 W cm^{-2}. **c** Droplet position relative to the center of the light pattern versus time for the 48-μm radius droplet from (**b**). **d** Induced force on droplets as a function of time for various light intensities (light pattern radius: 64 μm, oil depth: 110 μm, droplet volume: 337 pl, and droplet radius: 43 μm). The initial distance between the droplet and the center of the light pattern is 235 μm (±5%). **e** Induced force on droplets as a function of time with various light pattern sizes. The light pattern is kept at the highest intensity of 13.53 W cm^{-2} (oil depth: 130 μm, droplet volume: 75 pl, and droplet radius: 26 μm). The initial distance between the droplet and the center of the light pattern is 200 μm (±5%)

after 0.6 s shows that the droplet slows down when it is trapped by the light pattern. One possible explanation for this is that the droplet, initially positioned 200 μm from the center of the light pattern, is first pushed away from the light pattern, then recirculates and ends up moving back towards the light pattern in the sub flow. When the droplet approaches the light pattern, it is pushed upwards by the circulation, and re-enters the upper flow. This upper flow is shallower than 30% of the total oil depth, as the higher power associated with the larger light pattern increases the upper flow velocity over the nominal condition. Thus, the droplet has increased contact with the sub flow, and the net viscous force pulls the droplet towards the center of the circulation. This is the case for the droplet manipulated by the 113-μm radius light pattern. During the first 0.3 s, the droplet is pushed away by the upper flow from its initial position 200 μm away from the center of the light pattern. Between 0.3 and 0.8 s, the droplet circulates with the flow, and moves back towards the light pattern to re-enter the upper flow. At 0.88 s, the droplet reaches the region with an upper flow shallower than 30% of the oil depth, and begins to slow down and move towards the convection center.

Predicting whether a droplet can be trapped by optothermal circulation depends on the force on the droplet. Larger droplets have more contact with the sub flow, which pulls the droplet to the circulation center. The stronger the circulation, the larger viscous force that is imparted to the droplet. However, the z-component of a circulation that is too strong will push the droplet to the substrate, making it move slower due to friction. If the radius of the droplet of interest can be kept between 30 and 50% of the oil depth and the circulation can be kept within certain range, such as when the light intensity is smaller than 12.8 W cm^{-2} in Fig. 4d, the droplet will not contact the substrate, and will be captured more readily by the optothermal circulation.

It should also be noted that surfactant aggregation at the trailing edge of the oil/water interface causes the solutal Marangoni effect to cancel out the thermocapillary effect at the same interface (Dixit et al. 2010), resulting in no significant net fluid motion. Thus, droplet manipulation experiments performed in enclosed chambers, which have no oil/air interface, resulted in no net droplet movement, as there is no additional interface that produces thermocapillary flow.

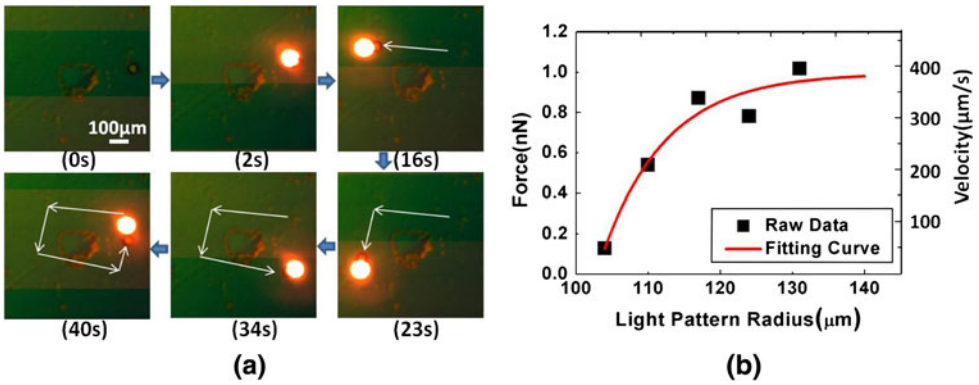

Fig. 5 Single droplet optothermal manipulation. **a** A 75-pl (radius: 26 μm) droplet is moved around a feature on the substrate surface (center of images). Photos are arranged clockwise. The oil depth is 100 μm. **b** The relation between the droplet (volume: 151 pl, radius: 33 μm) force and velocity as a function of the light pattern size (oil thickness: 210 μm). An exponential trendline has been added to the graph

4.2 Single droplet manipulation

The manipulation of a single 75-pl droplet (radius: 26 μm) is demonstrated (Fig. 5a). The droplet movement is controlled in four directions, forming a rectangular trajectory around a stationary feature on the substrate surface.

To increase the manipulation velocity, stronger circulation is needed. Figure 5b shows the force induced by different light patterns on the droplet (volume: 151 pl, radius: 33 μm) as the droplet is transported by the light pattern. The data are obtained using different light patterns to drag the droplet at the highest possible velocity. The force is calculated from the velocity data using Stokes' Law. The force curve starts at the point when the light pattern is strong enough to induce droplet trapping, and ends when the induced circulation causes the droplet to contact and stick to the substrate.

Larger light patterns can be used to generate a stronger circulation to transport droplets at faster rates. For example, in Fig. 5b, the 110-μm radius light pattern provides a force of 0.54 nN, which means that a 151-pl droplet can be transported at a rate of 211 μm s^{-1}. In contrast, when the light pattern radius is increased to 117 μm, the circulatory flow can provide a force of 0.87 nN, while moving the droplet at 342 μm s^{-1}.

In this case, faster droplet manipulation requires a stronger circulation to produce more force on the droplets. However, if the oil depth is kept constant, a stronger circulation will push the droplet closer to the substrate, as discussed in the characterization section, which results in slower droplet movement. In Fig. 5b, when the light pattern radius is larger than 131 μm, the circulation becomes strong enough that the droplet/surface interaction causes the droplet to cease movement in response to a translated light pattern. Thus, to achieve an increased droplet velocity, thicker oil should be used in conjunction with increased circulatory flow.

By adjusting oil depth, light pattern properties such as size and intensity, and the rate of the light pattern translation, a suitable circulation profile can be achieved to trap and transport droplets with volumes greater than 10 pl (radius: 13 μm). Increasing light pattern intensity and size results in increased manipulation velocities, but intense light patterns may not be preferable since they can reduce the reliability of the manipulation. Larger light patterns heat up the oil layer more, resulting in faster evaporation of oil and droplets. In addition, since a static light pattern can create a stronger circulation than that generated by a moving pattern, when a large light pattern ceases movement during the manipulation, the instantaneous sub flow velocity cannot sustain the upper flow velocity, which is strong enough to deplete the oil layer and alter the air/oil interface, affecting the manipulation environment.

One way to achieve efficient droplet manipulation for single droplet manipulation is to use smaller, less intense light patterns to trap droplets, and use larger, more intense light patterns when transporting droplets.

4.3 Droplet fusion and multiple droplet manipulation

One essential function of a droplet system is the merging of droplets. This was demonstrated using two droplets containing different dyes (Fig. 6). Two 270-pl (radius: 40 μm) droplets, one with a blue dye, and the other with a red dye, represent microreactors containing different reagents. Before turning on the light pattern, 1 μl of destabilizer solution was added to the open chamber to reduce the effect of surfactants. Light patterns were created close to the target droplets. Droplets immediately moved towards the light patterns and fused into one 533-pl (radius: 50 μm) droplet. To provide a fusion force as large as possible, the

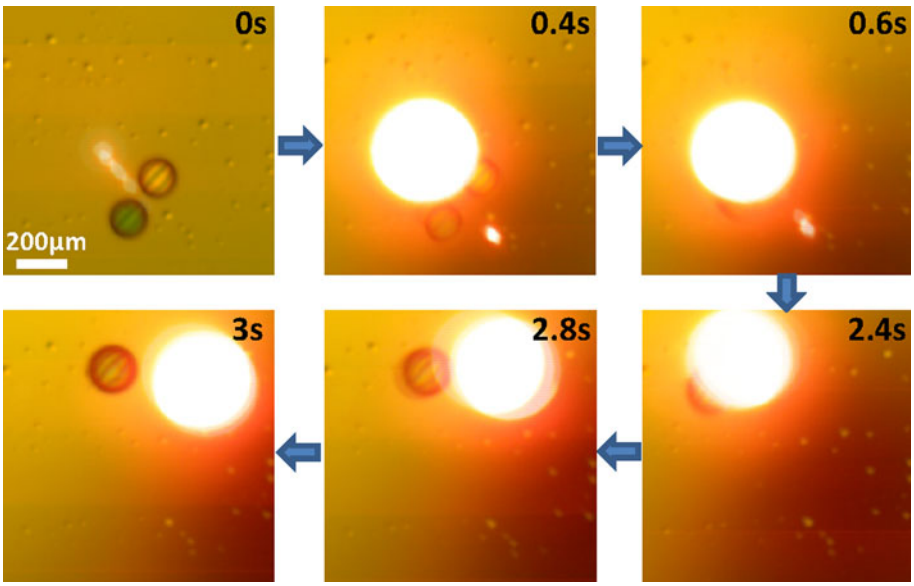

Fig. 6 Two discrete 270-pL droplets (radii: 40 μm), one loaded with *red* dye (lighter colored droplet), and the other loaded with *blue* dye (darker colored droplet), are merged by projected light patterns. The droplets filled with *blue* and *red* dye appear to be *green* and *yellow*, respectively, as they are viewed using differential interference contrast microscopy. Complete mixing of the dyes is observed at the conclusion of the droplet manipulation

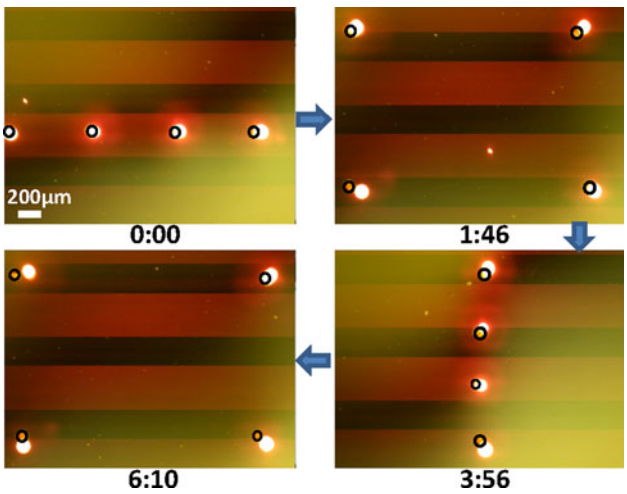

Fig. 7 Four droplets are manipulated in parallel into different formations. Droplet positions are indicated by the *black* circles. *Horizontal stripes* in the images are artifacts caused by a mismatch between the frame rates of the projector and camera

light patterns used here are at an intensity of 13.53 W cm^{-2}, with a radius of 107 μm, enclosing the two droplets. The axisymmetric nature of the circulatory force facilitates the merging of droplets. The two droplets fuse in less than 1 s. Loss of fluid during the fusion is negligible. Due to the rotation induced by the torque, the resultant droplet displays rapid mixing, with an evenly distributed color between blue and red.

Another important function is the simultaneous manipulation of multiple droplets (Fig. 7). Here, each droplet with an average volume of 671 pl (radius: 54 μm) is moved individually by direct user control, while other droplets are anchored in place by other light patterns. The light patterns used here are created by customized computer code. The light patterns are at an intensity of 13.53 W cm^{-2}, and their radii are controlled to be less than 50 μm to prevent overheating and oil depletion. This process can be easily modified to enable automated parallel manipulation of multiple droplets. These droplets are transported at an average velocity of 100 μm s^{-1}.

Parallel droplet manipulation adds further complexity to droplet control. One concern is inadvertently affecting the trajectory of a droplet by the light pattern used to control an adjacent droplet. To quantify this, we define the resolution of the optothermal manipulation to be the minimum lateral separation necessary so that the trajectory of a droplet being transported at highest possible velocity does not deviate by more than a droplet radius when moved next to another light pattern (Fig. 8a). The resolution of individual droplet manipulation does not change significantly as the light pattern radius increases (Fig. 8b). Although stronger circulatory flow is associated with larger scale, this stronger flow also provides more force to trap a droplet in a fixed location. These two effects nearly cancel out each other, resulting in an average resolution of 146.5 μm for droplets with a volume of 47 pl (radius: 22 μm). However, this does not mean that larger light patterns are always better for manipulation. As discussed above, larger light patterns heat the substrate more, and can lead to droplet evaporation and depletion of the oil layer. Thus, in order to maintain efficient control of individual droplets, the light patterns should be kept within certain range. In the experimental setups presented here, 50 μm is a preferred upper limit for light pattern radius in parallel droplet manipulation.

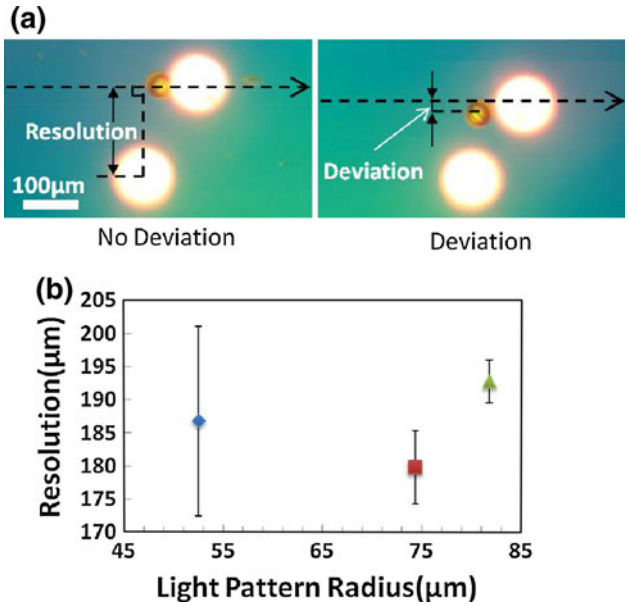

Fig. 8 Relation between resolution and light pattern radius (droplet volume: 47 pl, radius: 22 μm, and oil depth: 130 μm). **a** The resolution is defined as the minimum separation necessary between the centers of adjacent light patterns such that the trajectory of a transported droplet deviates by less than one droplet radius. **b** Measured resolution as a function of light pattern radius

5 Conclusion

Microscale circulation generated by Marangoni forces is well suited as a tool for nano- and pico-liter droplet manipulations. Here, we have demonstrated the trapping and transportation of droplets by optically inducing circulatory flows using an optically absorbing substrate and a computer projector. To the best of our knowledge, this is the first demonstration of optically induced thermal droplet manipulation using an incoherent source. Droplets with volumes ranging from 44 to 671 pl (radii: 22 to 54 μm) were manipulated at velocities of up to 400 μm s^{-1}, corresponding to forces of up to 1 nN. The induced force on droplets also has a size dependence, which could be possibly exploited for selecting droplets of a particular size. Future study will include using a feedback loop to automate the whole manipulation process, including the modulation of the light pattern in real time to optimize circulation profiles during manipulation.

Acknowledgments This project is funding in part by the National Science Foundation, grant number EEC09-26632. The authors would like to thank Dr. Yi Zuo for assistance with surface tension measurements.

References

Basu AS, Gianchandani YB (2009) A programmable array for contact-free manipulation of floating droplets on featureless substrates by the modulation of surface tension. J Microelectromech Syst 18(6):1163–1172

Batchelor GK (2000) An introduction to fluid dynamics. Cambridge University Press, Cambridge

Chiou PY, Park SY, Wu MC (2008) Continuous optoelectrowetting for picoliter droplet manipulation. Appl Phys Lett 93(22):221110

Choi CH, Jung JH, Rhee Y, Kim DP, Shim SE, Lee CS (2007) Generation of monodisperse alginate microbeads and in situ encapsulation of cell in microfluidic device. Biomed Microdev 9(6):855–862

COMSOL Multiphysics (2008) Marangoni circulation, COMSOL Multiphysics User Manual. pp 391-402

Cordero ML, Bumham DR, Baroud CN, McGloin D (2008) Thermocapillary manipulation of droplets using holographic beam shaping: microfluidic pin ball. Appl Phys Lett 93(3):034107

Cordero ML, Rolfsnes HO, Burnham DR, Campbell PA, McGloin D, Baroud CN (2009) Mixing via thermocapillary generation of flow patterns inside a microfluidic drop. New J Phys 11(9):075033

Cygan ZT, Cabral JT, Beers KL, Amis EJ (2005) Microfluidic platform for the generation of organic-phase microreactors. Langmuir 21(8):3629–3634

Darhuber AA, Valentino JP, Davis JM, Troian SM, Wagner S (2003) Microfluidic actuation by modulation of surface stresses. Appl Phys Lett 82(4):657–659

Di Carlo D (2009) Inertial microfluidics. Lab Chip 9(21):3038–3046

Dixit SS, Kim H, Vasilyev A, Eid A, Faris GW (2010) Light-driven formation and rupture of droplet bilayers. Langmuir 26(9):6193–6200

Emilie V, Cordero ML, Gallaire F, Baroud CN (2009) Laser-induced force on a microfluidic drop: origin and magnitude. Langmuir 25(9):5127–5134

Eötvös R (1886) Ueber den zusammenhang der oberflächenspannung der flüssigkeiten mit ihrem molecularvolumen. Ann Phys 263(3):448–459

Farahi RH, Passian A, Ferrell TL, Thundat T (2005) Marangoni forces created by surface plasmon decay. Opt Lett 30(6):616–618

Farahi RH, Rassian A, Zahrai S, Lereu AL, Ferrell TL, Thundat T (2006) Microscale Marangoni actuation: all-optical and all-electrical methods. Ultramicroscopy 106:815–821

Higuera FJ (2000) Steady thermocapillary-buoyant flow in an unbounded liquid layer heated nonuniformly from above. Phys Fluids 12(9):2186–2197

Holden MA, Needham D, Bayley H (2007) Functional bionetworks from nanoliter water droplets. J Am Chem Soc 129(27):8650–8655

Holtze C, Rowat AC, Agresti JJ, Hutchison JB, Angilè FE, Schmitz CHJ, Köster S et al (2008) Biocompatible surfactants for water-in-fluorocarbon emulsions. Lab Chip 8(10):1632–1639

Hur SC, Tse HTK, Di Carlo D (2010) Sheathless inertial cell ordering for extreme throughput flow cytometry. Lab Chip 10(3):274–280

Kotz KT, Noble KA, Faris GW (2004) Optical microfluidics. Appl Phys Lett 85(13):2658–2660

Lereu AL, Passian A, Farahi RH, Zahrai S, Thundat T (2006) Plasmonic Marangoni forces. J Eur Opt Soc Rapid Publ 1:06030

Luo C, Yang X, Fu Q, Sun M, Ouyang Q, Chen Y, Ji J (2006) Picoliter-volume aqueous droplets in oil: electrochemical detection and yeast cell electroporation. Electrophoresis 27(10):1977–1983

Neale SL, Ohta AT, Hsu HY, Valley JK, Jamshidi A, Wu MC (2009) Trap profiles of projector based optoelectronic tweezers (OET) with HeLa cells. Opt Express 17(7):5232–5239

Palit R (1956) Thermodynamic interpretation of the Eötvös constant. Nature 177(4521):1180

Park SY, Pan CL, Wu TH, Kloss C, Kalim S et al (2008) Floating electrode optoelectronic tweezers: light-driven dielectrophoretic droplet manipulation in electrically insulating oil medium. Appl Phys Lett 92(15):151101

Park S, Teitell MA, Chiou PY (2010) Single-sided continuous optoelectrowetting (SCOEW) for droplet manipulation with light patterns. Lab Chip 10(13):1655–1661

Passian A, Zahrai S, Lereu AL, Farahi RH, Ferrell TL, Thundat T (2006) Nonradiative surface plasmon assisted microscale Marangoni forces. Phys Rev E 73(6):066311

Schwartz JA, Vykoukal JV, Gascoyne PRC (2004) Droplet-based chemistry on a programmable micro-chip. Lab Chip 4(1):11–17

Selva B, Miralles V, Cantat I, Jullien MC (2010) Thermocapillary actuation by optimized resistor pattern: bubbles and droplets displacing, switching and trapping. Lab Chip 10(14):1835–1840

Solvas XCI, Srisa-Art M, Demello AJ et al (2010) Mapping of fluidic mixing in microdroplets with 1 μs time resolution using fluorescence lifetime imaging. Anal Chem 82(9):3950–3956

Song H, Chen DL, Ismagilov RF (2006) Reactions in droplets in microfluidic channels. Angew Chem Int Ed 45(44):7336–7356

Srinivasan V, Pamula VK, Fair RB (2004) An integrated digital microfluidic lab-on-a-chip for clinical diagnostics on human physiological fluids: the science and application of droplets in microfluidic devices. Lab Chip 4(4):310–315

Zagnoni M, Cooper JM (2010) A microdroplet-based shift register. Lab Chip 10(22):3069

Zhao Y, Fang J, Wang H, Wang X, Lin T (2010) Magnetic liquid marbles: manipulation of liquid droplets using highly hydrophobic Fe_3O_4 nanoparticles. Adv Mater 22(6):707–710

Zuo YY, Do C, Neumann AW (2007) Automatic measurement of surface tension from noisy images using a component labeling method. Colloids Surf A 299:109–116